Lawrence Berkeley National Laboratory

Title
Phase Control on Surface for the Stabilization of High Energy Cathode Materials of Lithium Ion Batteries

Permalink
https://escholarship.org/uc/item/0829p6nj

Journal

ISSN

Authors
Piao, Jun-Yu
Gu, Lin
Wei, Zengxi
et al.

Publication Date

DOI

Peer reviewed

Phase Control on Surface for the Stabilization of High Energy Cathode Materials of Lithium Ion Batteries

Jun-Yu Piao[1,2], Lin Gu[2,3], Zengxi Wei[4], Jianmin Ma[4], Jinpeng Wu[5,6], Wanli Yang[5], Yue Gong[2,3], Yong-Gang Sun[1,2], Shu-Yi Duan[1,2], Xian-Sen Tao[1,2], De-Shan Bin[1,2], An-Min Cao*[1,2], Li-Jun Wan[1,2]

1. CAS Key Laboratory of Molecular Nanostructure and Nanotechnology, Institute of Chemistry, Chinese Academy of Sciences (ICCAS), Beijing 100190, China.
2. University of Chinese Academy of Sciences (UCAS), Beijing 100049, China.
3. Beijing National Laboratory for Condensed Matter Physics, Institute of Physics, Chinese Academy of Sciences (CAS), Beijing 100190, China.
4. College of Physics and Electronics, Hunan University, Changsha 410022, China.
5. Advanced Light Source, Lawrence Berkeley National Laboratory, Berkeley, CA 94720, USA.
6. Geballe Laboratory for Advanced Materials, Stanford University, Stanford, CA 94305, USA.

Supporting Information Placeholder

ABSTRACT: The development of high energy electrode materials for lithium ion batteries is challenged by their inherent instabilities, which become more aggravated as the energy densities continue to climb, accordingly causing increasing concerns on battery safety and reliability. Here, taking the high voltage cathode of $LiNi_{0.5}Mn_{1.5}O_4$ as an example, we demonstrate a protocol to stabilize this cathode through a systematic phase modulating on its particle surface. We are able to transfer the spinel surface into a 30 nm shell composed of two functional phases including a rock-salt one and a layered one. The former is electrochemically inert for surface stabilization while the latter is designated to provide necessary electrochemical activity. The precise synthesis control enables us to tune the ratio of these two phases, and achieve an optimized balance between improved stability against structural degradation without sacrificing its capacity. This study highlights the critical importance of well-tailored surface phase property for the cathode stabilization of high energy lithium ion batteries.

Rechargeable Lithium ion batteries (LIBs) have enabled the wide use of the portable electronics and shown promising potential in electric vehicles.[1-3] Accordingly, high energy electrode materials, particularly cathode ones which are the determining factor for the energy density of LIBs, are being urgently pursued for the applications of next generation LIBs.[4] However, along with the continuous climbing of the energy density of cathode materials, which are usually characterized by its high capacity or high working voltage, the unstable cathode/electrode interface become a serious concern.[3] It has been widely documented that fully-delithiated cathode materials are highly active when exposed to flammable organic electrolytes, resulting in chemical and mechanical instability of the electrode.[5] Particularly, the parasitic side reactions and transition metal (TM) dissolution will exacerbate at high energy density, which can provoke severe structural degradation of the cathode materials with high risk for capacity loss and thermal runaway, which draw increasing concerns on the battery safety and reliability.[5,6] Therefore, it is of paramount importance that cathode materials can be designed and engineered for stability control before they can be possibly considered for practical use in high energy LIBs.

To achieve a stable cathode, it is reasonable to expect that surface medication be very effective since the structural degradation is initiated right from the electrode/electrolyte interface reactions.[7,8] Accordingly, surface coating of cathode materials by an electrochemically-inert species such as Al_2O_3 become favorable, which can act as a protective shell to suppress side reactions and TM dissolution at the electrode-electrolyte interface, and provide a stable surface benefiting from the inertness of the coating layer.[5,6,9] However, the inert surface would lead to a sluggish Li^+ and electron diffusion, easily resulting in an increased impedance and deteriorated rate performance.[6,10] Meanwhile, recent development showed that surface cationic

substitution could be helpful for the surface stabilization of different cathode materials.[11] An representative work by Lu et al. showed that a partial replacement of Mn by Ti on the surface of $LiMn_2O_4$ was able to change the surface chemistry, which could ensure an improved interfacial stability beneficial for the structural stability of the cathode materials upon long cycles.[11]

In this communication, we will identify an effective stabilization strategy for high energy cathode materials through a systematic engineering of the surface phase properties. Taking $LiNi_{0.5}Mn_{1.5}O_4$ (LNMO) as an example, which is a high energy cathode material and well-known for its dilemma between high working voltage (4.7 V from $Ni^{2+/3+}$ and $Ni^{3+/4+}$ redox couples) and its proneness for structure degradation during cycling,[6,12] we are able to initiate a controlled phase transition on the particle surface, and transfer its spinel structure into a mixture of two functional phases with well-tailored surface chemistry. Specifically, ZnO is used to react with LNMO right on the surface of the cathode particles with the amount of ZnO precisely controlled. Such a surface reaction forms a 30 nm biphasic layer including a rock-salt one and a layered one without changing the underneath spinel structure. The rock-salt like phase contains a high Zn^{2+} content and its electrochemical inertness is suitable for surface stabilization. Meanwhile, the surface domains with a layered-like structure are designated as channels for charge transfer, which are critical to ensure a high electrochemical performance of the LNMO cathode. Our synthesis control enabled us a capability to precisely tune the ratio of these two phases right on the particle surface, and achieve an optimized balance between improved stability against structural degradation while without sacrificing its capacity. Our experimental data and theoretical simulations confirmed that such a phase modulation was high favorable in surface chemistry for the stabilization of the high energy LNMO cathode.

To control the surface properties, we firstly built a uniform ZnO coating layer around each LNMO particle whose shell thickness could be precisely controlled, and then the particles were heated at higher temperatures to intrigue the surface structural transformation. Notably, the accurate control of the ZnO layer endowed us a good model system with surface properties strictly defined for a systematic investigation the change in the surface chemistry of the prepared cathode materials. Figure 1a showed a transmission electron microscopy (TEM) image of the pristine LNMO particles we have used, which were prepared through a sol-gel protocol and had a particle size around 2 μm.[13] The high resolution TEM (HRTEM) image of the particle surface revealed a free borderline on these LNMO particles. Following our newly-developed protocol (seeing supporting information for experimental details), a uniform coating layer of ZnO could be grown around each LNMO particle. Figure 1b showed a representative TEM image of the ZnO-coated LNMO particles. There clearly existed a uniform surface layer with its thickness around 4 nm as further confirmed by the HRTEM analysis in the inset of Figure 1b. The elemental mapping (Figure 1c-f) of

a randomly-selected particle revealed the homogeneously dispersion of Zn on the LNMO surface, confirming the formation of a core-shell structure with a continuous and conformal ZnO coating layer around the LNMO particle. Meanwhile, by changing the synthesis parameters, we can tune the thickness of the surface LNMO layers from 2 nm to over 20 nm (Figure S1) for further heat treatment.
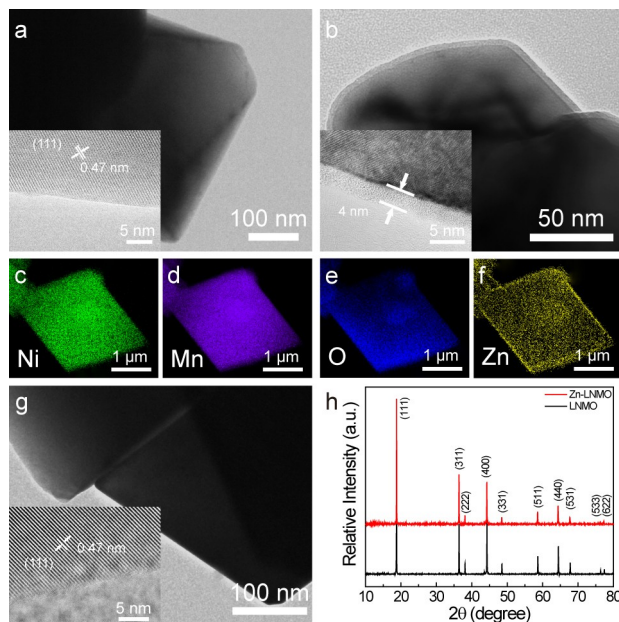

Figure 1. (a) TEM image of a pristine LNMO sample which has a clean surface. The inset is its corresponding HRTEM image, which shows a lattice spacing of 0.47 nm for the spinel (111) planes. **(b)** TEM image of LNMO@ZnO. The inset HRTEM image shows an amorphous coating layer with a thickness of around 4 nm. **(c-f)** Elemental mappings for Ni, Mn, O, and Zn, respectively, for a randomly-selected LNMO@ZnO particle. Zn exists uniformly on the surface. **(g)** TEM image of the annealed Zn-LNMO sample. The coating layer vanishes as shown in the inset HRTEM image. The lattice spacing remained at 0.47 nm. (h) XRD spectra of LNMO and Zn-LNMO. Both show a spinel structure with the space group of *Fd-3m*.

The surface ZnO layer would disappear upon the following annealing process at 700°C for 2 hours. As shown in Figure 1g, the sample surface turned smooth with no outer shell observed (sample denoted as Zn-LNMO), revealing the existence of solid reaction between ZnO and its underneath LNMO particle caused by the high temperature treatment. The analysis of X-ray photoelectron spectroscopy (XPS) confirmed the existence of Zn^{2+} on the surface of Zn-LNMO (Figure S2a), while the HRTEM characterization (inset in Figure 1g) showed no obvious change on the crystalline structure of the LNMO particle according to the measured lattice spacing for its (111) plane (inset in Figure 1g). The X-ray diffraction (XRD) pattern for Zn-LNMO was almost the same as that for the pure LNMO one (Figure 1h). Both shows a typical spinel phase (PDF#80-2162) and indicates that the surface treatment would not cause noticeable change on the bulk spinel structure. The elemental analysis by using inductively-coupled plasma atomic emission

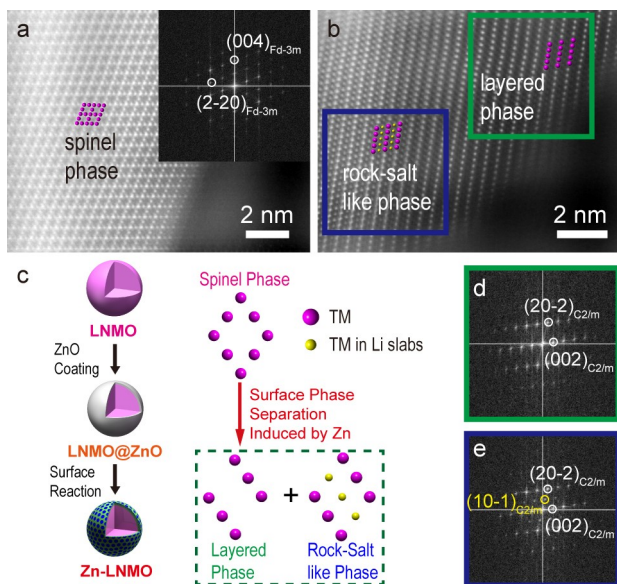spectroscopy (ICP-AES) showed that the amount of Zn was 1.20 wt% in the Zn-LNMO.

Figure 2. (a) STEM-HAADF image for the surface structure of LNMO. The inset is its reduced FFT image, showing a standard spinel structure. **(b)** STEM-HAADF image for the surface structure of Zn-LNMO, which shows the coexistence of two different phases including a rock-salt like one (in blue square) and a layered one (in green square). **(c)** Schematic diagram to describe the surface control procotol. The surface solid reaction can introduce Zn^{2+} into the spinel lattice, resulting in a phase transformation process to form a biphasic surface layer. **(d)** Reduced FFT image of the layered region (in green square) in panel b. **(e)** Reduced FFT image of the rock-salt like region (in blue square) in panel b. The emergence of $(10\text{-}1)_{C2/m}$ spots indicates the formation of the rock-salt like phase.

Intrigued by the disappearance of the ZnO layer on the surface of Zn-LNMO, we tried further characterizations assisted by the aberration-corrected scanning TEM under a high-angle angular dark-field (STEM-HAADF) mode, which was able to provide the atomic scale images of heavy elements.[14] Figure 2 recorded the STEM-HAADF images on the surfaces of the two concerned samples, namely LNMO and Zn-LNMO, along the spinel [110] crystallographic direction. Diamond-shaped patterns could be observed for the pristine sample (Figure 2a), which were in good consistence with a typical spinel structure.[15] The extracted reduced fast Fourier transformed (FFT) pattern (inset in Figure 2a) showed ordering spots corresponding to space group of *Fd*-3*m*. Interestingly, the solid reaction on the surface resulted in a striking change on the atomic arrangement. For the Zn-LNMO particle, although the bulk phase remained spinel, such a structural character no longer existed on the surface and a biphasic layer emerged instead with a depth around 30 nm. As shown in Figure 2b, two distinct types of crystalline structures prevailed on the surface as marked in the squares, whose atom columns were arranged in styles showing typical features of a rock-salt like phase (blue square) together with a layered one (green square). It was

noted that all the three concerned structures belonged to the same subgroup of O3 phase originated from a cubic-close-packed array of oxygen.[10] The subtle difference among these three types could be partially visualized by the reduced FFT analysis. Particularly, the Li slabs of the *C*2/*m* phase from the layered structure (Figure 2d) could be partially occupied by heavy cation, forming a rock-salt like phase as highlighted by those $(10\text{-}1)_{C2/m}$ spots in the reduced FFT pattern (Figure 2e).[16]

To have a better understanding on these two newly-emerged phases on the surface, we performed the energy dispersive X-ray emission spectroscopy (EDS) analysis to probe the chemical compositions of different nanodomains. We found that the atom ratios of Ni/Mn remained at a nearly-constant value of 1:3 for different tested locations on the surface including those nanodomains for the rock-salt like phase and its layered counterpart (Table S2). Meanwhile, we did notice an obvious difference when the Zn contents were examined. The rock-salt like phase showed a higher Zn^{2+} content than that in the layered phase. Furthermore, we were able to increase the Zn content on the surface by introducing a much thicker ZnO coating layer (13 nm) for the surface solid reaction (Figure S3a). After sintering, the final product (denoted as 13-Zn-LNMO) were dominated by rock-salt like phase on the surface with few layered ones observed. The contrast of the columns located in Li slabs of the *C*2/*m* phase became much brighter than observed in Zn-LNMO, showing a higher TM filling fraction in the Li slabs of the *C*2/*m* phase with higher Zn content. Unfortunately, due to the technique challenge, it was not possible for us to identify single Zn atoms inside the lattice. The electron energy loss spectroscopy (EELS) had been widely used for single atom identification. But its signal for Zn existed as small bump with low intensity due to the technical nature, making it impossible for us to locate Zn in the structure as usually do for other elements. However, considering the constant Ni/Mn ratio in the two coexistent phases as well as the smooth transition between these two as shown in Figure 2b, we expected that those excess Zn^{2+} mainly enriched in the Li slabs so that a further increase of Zn^{2+} would result in a direct increase of the rock-salt like phase at the expense of the layered domains. To describe the whole process mentioned above, Figure 2c schemed the whole structural change on the LNMO surface, which featured the phase transition from the spinel one to a biphasic character.

The obvious change in the surface structure from different ZnO shells inspired us to do a systematic modulation of the surface chemistry through the synthesis control. As a matter of fact, a capability to perceive the delicate change on the surface is largely dependent on the synthesis capability, through which we managed to precisely control the amount of Zn^{2+} used for solid reaction and succeeded in providing surfaces with specific surface properties for a reliable structural identification at an atomic level. Otherwise, for samples based on either a mixture of ZnO and LNMO or ununiform ZnO coatings, the detail change of the structural information in nanodomains could be

easily overlooked and became a challenging task for researchers to track and identify the structural evolution on surface. Our precise surface control together with the corresponding STEM-HAADF analysis on the prepared Zn-LNMO products clearly revealed a gradual change of the biphasic surface chemistry. After the surface reaction, structural transformation originated from spinel was observed and a layered phase was more prominent at relatively lower Zn^{2+} content (Figure 3a). In responding to higher Zn^{2+} content, the rock-salt like phase gradually increase its portion, probably due to the occupation of Zn^{2+} in the Li slabs of the layered phase (Figure 3b). Accordingly, further increase of the Zn^{2+} content would lead to an extremely high TM occupation ratio in Li slabs, showing a much higher contrast in Li slabs in STEM-HAADF image (Figure 3c). Figure 3d schemed the gradual phase change on the surface in response to the Zn^{2+} content in nanodomains, which highlighted a flexible capability to tune the surface composition through our synthesis control on the LNMO surface.
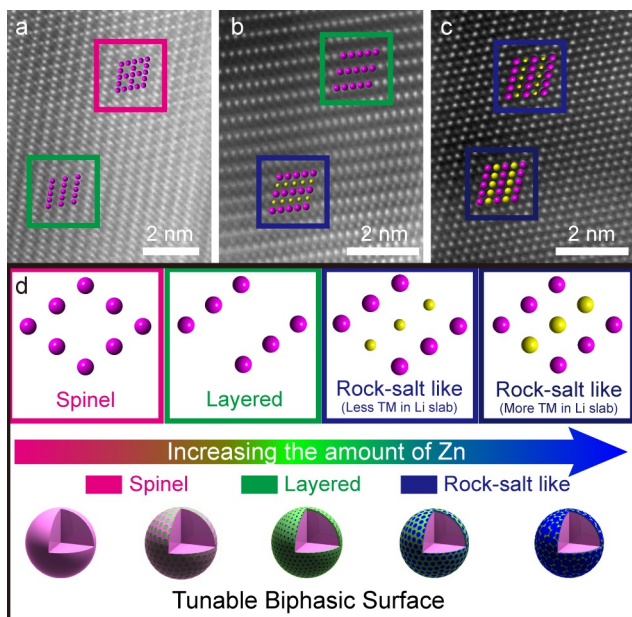

Figure 3. (a-c) STEM-HAADF images to show the surface structure of samples with the increase of Zn content. **(a)** Coexistence of a spinel phase and a layered phase. **(b)** Coexistence of the layered phase and the rock-salt like phase. **(c)** Surface dominated by rock-salt like phase at high Zn content. **(d)** Schematic illustration for the phase evolution observed on LNMO surface in respond to the change in Zn content. The spinel surface will be transformed into different phases with a highly tunable phase ratios, which highlights a gradual increase of the rock-salt phase in the biphasic layer until its dominance on the surface at high Zn content.

Our pursuit on surface engineering of LNMO particles was motivated by the critical role played by surface chemistry on the structural stability and performance reliability of high energy cathode.[5,8] After controlling the surface structures, we studied the cell performance of these LNMO samples in aim of achieving a fundamental understanding towards optimized design of suitable surface for stable cathodes. Figure 4a compared the charge/discharge

curves of representative samples including the pristine LNMO and the Zn-LNMO ones with different Zn contents. All these samples showed the characteristic plateaus around 4.7 V originated from the redox couples of both $Ni^{2+/3+}$ and $Ni^{3+/4+}$.[12] For the Zn-treated samples, we didn't observe obvious change in its charge/discharge profiles at lower Zn contents. For example, the Zn-LNMO showed almost the same curves as those of LNMO, indicated that the existence of small amount of Zn on the surface didn't have noticeable impact on the intrinsic property of the LNMO sample during the insertion/desertion of Li^+. However, a higher Zn content as observed on 13-Zn-LNMO delivered much lower specific capacity with deformed charge/discharge profiles, showing that the cell performance was highly dependent on the Zn^{2+} content. The most prominent contribution from the surface treatment was found to be the much improved cycling stability. After 100 cycles, the pristine sample showed severe decay in specific capacity from 131.8 mAh/g to 121.4 mAh/g together with obvious change in plateau voltage, which was probably related to the aggravated polarization after long cycling.[17] In sharp contrast, the Zn-LNMO remained an almost unchanged capacity at 132.9 mAh/g after 100 cycles, showing a much better cycling stability of Zn-LNMO during the electrochemical process. Figure 4b compared the cycling performance of these LNMO-based samples at multiple cycling stages. An enhanced cycling stability could be achieved after the surface treatment but an optimized Zn^{2+} content was expected if the deliverable capacity was considered. In particular, a relatively less Zn^{2+} content (sintering the LNMO@2 nm ZnO at 700°C, denoted as 2-Zn-LNMO) was not adequate for surface protection and an extremely high Zn^{2+} content would result in the intolerable decrease in specific capacity. Figure 4c showed the rate capability for these samples, revealing a similar tendency related to the Zn-content. Interestingly, the Zn-LNMO sampled delivered a much higher capacity at 10 C, indicated that a biphasic surface of LNMO actually did not jeopardize the charge transfer of the cathode.

To understand the kinetics of the electrodes better, we carried out further test to probe the electrochemical interface assisted by the electrochemical impedance spectrum (EIS). An obvious increase in resistance (210.7 Ω) was observed for the pristine LNMO sample after 100 cycles, showing an interface deterioration process probably related to the surface reactions.[18] On the contrary, the Zn-LNMO sample showed an evident capability to alleviate such a deterioration process with a much reduced increase in impedance (27.1 Ω). The systematic EIS tests on different samples revealed a close relationship between the interface impedances of the prepared cells and the surface Zn^{2+} contents. Lower Zn^{2+} contents (2-Zn-LNMO and Zn-LNMO) didn't impact the charge transfer to a large extent while we observed a much higher interphase impedance on 13-Zn-LNMO, which showed a trend in good agreement with the calculation we carried out on the chemical diffusion coefficient of Li^+ assisted by the help of cyclic

voltammetry (CV) test (Table S3). Combined with the STEM-HAADF characterizations on the surface structure, it was not surprising that the Li+ mobility became sluggish as Zn^{2+} continued to increase on the surface, which was characterized by more TM ions taking position of the Li slabs of $C2/m$ phase, forming a rock-salt like structure with less electrochemical activity due to the jammed transportation path for Li+. It turned out that the Zn content was critical for the charge transfer on the surface, which explained well the electrochemical performance of different samples especially when tested at high rate in Figure 4c.
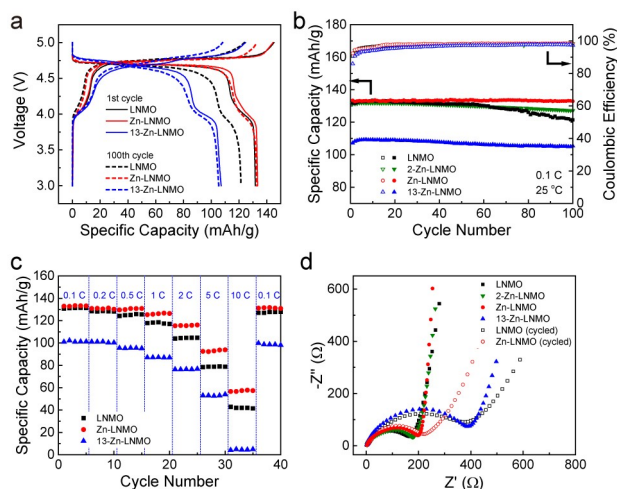

Figure 4. (a) Charge and discharge profiles during the 1st and 100th cycle at 0.1 C. **(b)** Cycling performance at 0.1 C. **(c)** Electrochemical performance at different rates. **(d)** Electrochemical Impedance Spectroscopy (EIS) spectra collected before cycling and after 100 cycles at 0.1 C with the frequency range of 0.1 Hz to 100 kHz.

We found that the surface modification caused significant changes on the stability of the LNMO sample. Differential scanning calorimetry (DSC) analysis showed that Zn-LNMO became more resistant against thermal-induced degradation (Figure S4a) with the much less heat released. Meanwhile, the sample after Zn treatment showed obvious advantage in high capacity retention and long-term cyclability when tested at elevated temperature (Figure S4b). Furthermore, we carried out ICP-AES test to investigate the Mn dissolution during cycling, which was considered as one of the major reasons for structure failure of the LNMO cathode.[19,20] Table S4 showed a clear trend that the modification in surface chemistry could effectively suppress Mn dissolution, which became more pronounced as the Zn concentration was further increased. Particularly, the 13-Zn-LNMO sample did not show obvious Mn loss after cycling, indicating a much improved structural stability of the cathode, which was actually not surprising to observe considering the fact that more rock-salt like phase took place on the surface and such a phase was more stable in nature.[21,22] Combined with the effect on the charge transfer, it was expected that a balanced control on the surface property became critical to ensure both a sufficient charge mobility and a much reduced Mn dissolution.

To directly confirm and unfold the stabilization mechanism of Zn-LNMO, we carried out surface analysis by employing synchrotron-based soft x-ray absorption spectroscopy (sXAS). sXAS is an electrochemical and chemical sensitive tool to characterize both transition-metals and oxygen states on battery electrode surface.[23,24] The purpose here is to compare the surface stability of the two comparative systems, LNMO and Zn-LNMO, after extended cycles, especially at high potential, i.e., charged state. We therefore focus on the total electron yield (TEY) data of sXAS, which is surface sensitive with probe depth of 10 nm. In general, for the electrodes before cycling, spectral difference between the LNMO and Zn-LNMO is negligible for all the Ni-L_3 (Figure 5a), Mn-L_3 (Figure 5b), and O-K (Figure 5c) edges. However, after 200 cycles, the electrodes at high potential (charged) display significantly different sXAS lineshape in all the edges. At the pristine and discharged states, the Ni-L_3 spectra display the typical Ni(II) lineshape in both systems, as expected.[12] The charged Zn-LNMO electrodes after 200 cycles show obvious lineshape signature of the Ni$^{2+/4+}$ redox, indicated by the enhanced Ni(IV) feature in charged states.[12] Note that, through such a surface sensitive probe, the strong Ni(II) peak at the charged states is from the top surface Ni(II) species, which has been previously reported in various Ni systems and are partially electrochemically inactive.[12,25,26] In sharp contrast, signatures of Ni(IV) completely disappear in the LNMO electrode at 200 cycle charged state, indicating a thick surface coating layer with electrochemically inactive Ni(II) species.[12] Consistently, the much stronger low energy feature in Mn-L_3 spectra of the LNMO at charged state, compared with Zn-LNMO, is from Mn(II) species, indicating again a very thick surface layer formation

or reconstruction for LNMO electrodes. We note that such a counterintuitive observation of surface coating with low-valence transition-metal species at high potentials is consistent with previous sXAS findings of high-voltage spinel electrodes due to electrolyte instability.[25] The strong surface formation effect at high potential for LNMO electrodes is again clearly seen in the O-*K* spectra, where the metal-oxygen hybridization features between 530-535 eV are largely suppressed, indicating the surface formation on LNMO is dominated by electrolyte decomposition products with features at high energies (535-545 eV).[25,26] The sharp contrast to the Zn-LNMO O-*K* sXAS signals could be seen again, where the spectrum maintains the overall lineshape, suggesting a relatively clean surface after 200 cycles. Therefore, the sXAS results on all the relevant elements consistently show that our Zn-LNMO electrode surface successfully suppressed the typical side reactions at high potentials, leading to a much more stable surface upon electrochemical cycling compared with LNMO. The data indicate a clean surface of the Zn-LNMO sample, which would benefit the convenient charge transfer on the electrode/electrolyte interface, in good agreement with our impedance test from the EIS analysis.
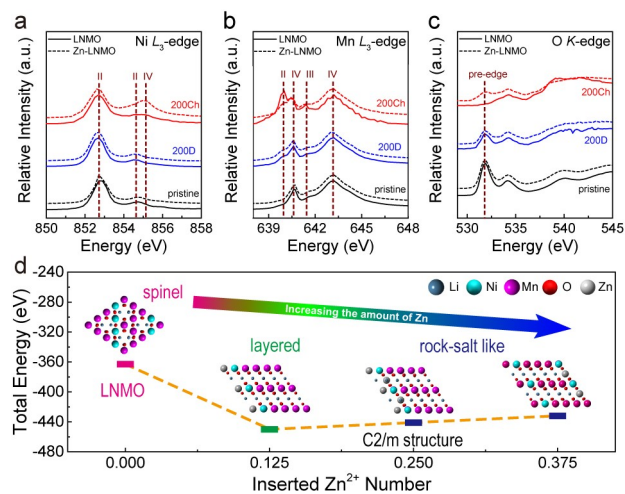

Figure 5. (a-c) sXAS TEY spectra of different electrodes tested before cycling and after 200 cycles at both charged state (200Ch) and discharged state (200D). **(a)** Ni *L*$_3$-edge sXAS spectra. After 200 cycles, the charged LNMO sample diminishes its Ni(IV) signal while a good retention is observed for Zn-LNMO. **(b)** Mn *L*$_3$-edge sXAS spectra. The spectra of LNMO electrode shows much stronger Mn(II) signal after 200 cycles. **(c)** O *K*-edge sXAS spectra. The pre-edge peak originated from the metal-oxygen hybridization is largely suppressed after 200 cycles for the LNMO electrode, but retains well for the Zn-LNMO one. Note the sXAS peak assignments in the figures are from previously established interpretation (see references in text). **(d)** The comparison of total energy between the structures with and without Zn^{2+}. The first-principles calculation has been used to determine the layered and rock-salt like structure with increasing amount of Zn^{2+}.

It was clear that the existence of Zn on the surface could effectively induce a controlled degree of phase separation on the surface, leading to a biphasic outside shell existing as a mixture of rock-salt like structure and a layered one with their phase ratio decided by the distribution of Zn. Starting from the solid state reaction at surface, it turned out that the insertion of Zn^{2+} into the spinel framework would lead to the formation of a more stable *C*2/*m* structure. The calculation by Cho et al. showed that the layered phase would become energetically more favorable than its spinel counterpart with the increase of the Li/TM ratio.[27] It seemed that the Zn^{2+} induced phase transition also proceeded towards the layered phase, which was interesting considering that Zn^{2+} (0.74 nm) had a similar ionic radii as Li$^+$ (0.76 nm),[28] and the presence of Zn had been reported to be effective for stabilizing layered structure.[19,20] To have better understanding on the phase transition, we performed the first-principles calculation to determine the feasibility for the formation of the *C*2/*m* phase. For simplicity, we compared the total energy of the LNMO sample before and after the Zn^{2+} insertion. Different *C*2/*m* structures with increasing Zn contents had been took into account to compare their total energies. As shown in Figure 5d, it was noteworthy that a Zn^{2+} containing *C*2/*m* phase showed a much lower energy compared to the spinel structure, indicated that the layered structure was indeed a more energetically-favorable phase for the structural evolution from the original spinel type. Meanwhile, we also found that the increased amount of Zn^{2+} would not cause a drastic energy change for the *C*2/*m* phase, revealing the high flexibility of the *C*2/*m* structure to host a large amount of Zn^{2+} in responding to different thickness of ZnO nanoshell used for surface reaction, which was in good agreement with our experimental observation in surface control.

In summary, we report a conceptually different strategy to stabilize high energy cathode materials through a systematic engineering of the surface phase properties. Particularly, we are able to control the surface chemistry of the high voltage LNMO cathode, and transform its spinel surface into a 30 nm biphasic shell composed of two functional phases, in which a rock-salt like one is electrochemically inert for surface stabilization while the a layered one is designated to provide necessary electrochemical activity. Our precise synthesis control on surface enables us a capability to control the phase ratio on the surface, and accordingly achieve an optimized balance between a high structural stability and excellent electrochemical performance. Our study highlights the critical importance of well-tailored surface chemistry for the cathode stabilization of high energy lithium ion batteries.

ASSOCIATED CONTENT

Supporting Information

The supporting information includes the method section and supplementary figures and tables (PDF). This material is available free of charge via the Internet at http://pubs.acs.org.

AUTHOR INFORMATION

Corresponding Author

* anmin_cao@iccas.ac.cn

Notes

The authors declare no competing financial interests.

ACKNOWLEDGMENT

REFERENCES

(1) Whittingham, M. S. Chem. Rev. **2004**, 104, 4271.

(2) Tarascon, J. M.; Armand, M. Nature **2001**, 414, 359.

(3) Goodenough, J. B.; Kim, Y. Chem. Mater. **2010**, 22, 587.

(4) Kang, K. S.; Meng, Y. S.; Breger, J.; Grey, C. P.; Ceder, G. Science **2006**, 311, 977.

(5) Lee, K. T.; Jeong, S.; Cho, J. Accounts Chem. Res. **2013**, 46, 1161.

(6) Manthiram, A.; Chemelewski, K.; Lee, E.-S. Energy Environ. Sci. **2014**, 7, 1339.

(7) Zheng, J. M.; Gu, M.; Xiao, J.; Zuo, P. J.; Wang, C. M.; Zhang, J. G. Nano Lett. **2013**, 13, 3824.

(8) Ma, J.; Hu, P.; Cui, G. L.; Chen, L. Q. Chem. Mater. **2016**, 28, 3578.

(9) Qi, R.; Shi, J.-L.; Zhang, X.-D.; Zeng, X.-X.; Yin, Y.-X.; Xu, J.; Chen, L.; Fu, W.-G.; Guo, Y.-G.; Wan, L.-J. Sci. China Chem. **2017**, 60, 1230.

(10) Radin, M. D.; Hy, S.; Sina, M.; Fang, C.; Liu, H.; Vinckeviciute, J.; Zhang, M.; Whittingham, M. S.; Meng, Y. S.; Van der Ven, A. Adv. Energy Mater. **2017**, 1602888.

(11) Lu, J.; Zhan, C.; Wu, T.; Wen, J.; Lei, Y.; Kropf, A. J.; Wu, H.; Miller, D. J.; Elam, J. W.; Sun, Y. K.; Qiu, X.; Amine, K. Nature Commun. **2014**, 5, 5693.

(12) Qiao, R.; Wray, L. A.; Kim, J.-H.; Pieczonka, N. P. W.; Harris, S. J.; Yang, W. J. Phys. Chem. C **2015**, 119, 27228.

(13) Sun, Y. K.; Lee, Y. S.; Yoshio, M.; Amine, K. Electrochem. Solid State Lett. **2002**, 5, A99.

(14) Zhang, Y.; Su, Z.; Azad, A. K.; Zhou, W.; Irvine, J. T. S. Adv. Energy Mater. **2012**, 2, 316.

(15) Wu, Q.; Liu, Y.; Johnson, C. S.; Li, Y.; Dees, D. W.; Lu, W. Chem. Mater. **2014**, 26, 4750.

(16) Yan, P.; Nie, A.; Zheng, J.; Zhou, Y.; Lu, D.; Zhang, X.; Xu, R.; Belharouak, I.; Zu, X.; Xiao, J.; Amine, K.; Liu, J.; Gao, F.; Shahbazian-Yassar, R.; Zhang, J.-G.; Wang, C.-M. Nano Lett. **2015**, 15, 514.

(17) Oumellal, Y.; Rougier, A.; Nazri, G. A.; Tarascon, J. M.; Aymard, L. Nature Mater. **2008**, 7, 916.

(18) Gauthier, M.; Carney, T. J.; Grimaud, A.; Giordano, L.; Pour, N.; Chang, H.-H.; Fenning, D. P.; Lux, S. F.; Paschos, O.; Bauer, C.; Magia, F.; Lupart, S.; Lamp, P.; Shao-Horn, Y. J. Phys. Chem. Lett. **2015**, 6, 4653.

(19) Pieczonka, N. P. W.; Liu, Z.; Lu, P.; Olson, K. L.; Moote, J.; Powell, B. R.; Kim, J.-H. J. Phys. Chem. C **2013**, 117, 15947.

(20) Jarry, A.; Gottis, S.; Yu, Y. S.; Roque-Rosell, J.; Kim, C.; Cabana, J.; Kerr, J.; Kostecki, R. J. Am. Chem. Soc. **2015**, 137, 3533.

(21) Liu, W.; Oh, P.; Liu, X.; Myeong, S.; Cho, W.; Cho, J. Adv. Energy Mater. **2015**, 5, 1500274.

(22) Lin, F.; Markus, I. M.; Nordlund, D.; Weng, T. C.; Asta, M. D.; Xin, H. L. L.; Doeff, M. M. Nature Commun. **2014**, 5, 3529.

(23) Li, Q.; Qiao, R.; Wray, L. A.; Chen, J.; Zhuo, Z.; Chen, Y.; Yan, S.; Pan, F.; Hussain, Z.; Yang, W. J. Phys. D: Appl. Phys. **2016**, 49, 413003.

(24) Qiao, R.; Lucas, I. T.; Karim, A.; Syzdek, J.; Liu, X.; Chen, W.; Persson, K.; Kostecki, R.; Yang, W. Adv. Mater. Interfaces **2014**, 1, 1300115.

(25) Qiao, R.; Wang, Y.; Olalde-Velasco, P.; Li, H.; Hu, Y.-S.; Yang, W. J. Power Sources **2015**, 273, 1120.

(26) Qiao, R.; Liu, J.; Kourtakis, K.; Roelofs, M. G.; Peterson, D. L.; Duff, J. P.; Deibler, D. T.; Wray, L. A.; Yang, W. J. Power Sources **2017**, 360, 294.

(27) Longo, R. C.; Kong, F. T.; Kc, S.; Park, M. S.; Yoon, J.; Yeon, D. H.; Park, J. H.; Doo, S. G.; Cho, K. Phys. Chem. Chem. Phys. **2014**, 16, 11233.

(28) Shannon, R. D. Acta Crystallogr., Sect. A **1976**, 32, 751.

SYNOPSIS TOC